Available online at www.sciencedirect.com
SCIENCE DIRECT®
International Journal of Heat and Fluid Flow 26 (2005) 506–512
International Journal of HEAT AND FLUID FLOW
www.elsevier.com/locate/ijhff

Laminar flow resistance in short microtubes

D.J. Phares [a,*,1], G.T. Smedley [b], J. Zhou [b]

[a] Department of Mechanical Engineering, Texas A&M University, College Station, TX 77843-3123, USA
[b] Department of Research & Development, Glaukos Corporation, 26061 Merit Circle, Suite 101, Laguna Hills, CA 92653, USA

Received 7 July 2004; accepted 29 November 2004
Available online 7 January 2005

Abstract

We have measured the pressure drop for the flow of liquid through a series of short microtubes ranging from 80 to 150 μm in diameter with aspect ratios between $L/D = 2$ and $L/D = 5$. These dimensions were selected to resemble lumens of implantable microstents that are under consideration for the treatment of glaucoma. For physiologically relevant pressure drops and flow rates, we have determined that a fully-developed laminar pipe flow may be assumed throughout the microtube when $(L/D) > 0.20Re$, where Re is the Reynolds number based on the diameter, D, and L is the length of the tube. We have examined flow rates between 0.1 and 10 μL/s, corresponding to Reynolds numbers between 1 and 150. For smooth microtubes, no difference from macroscopic flow is observed for the tube sizes considered. However, flow resistance is found to be sensitive to the relative surface roughness of the tube walls.

1. Introduction

The flow of liquids through microtubes and microchannels is becoming increasingly important as the size of mechanical devices and biological and chemical sensors continues to shrink. This has prompted a series of recent investigations focusing on measuring the resistance to liquid flow through tubes (Mala and Li, 2000; Li et al., 2003; Brutin and Tadrist, 2003) and channels (Kulinsky et al., 1999; Ren et al., 2001) smaller than a few hundred microns in hydraulic diameter. A deviation from macroscopic flow behavior is expected to occur in micron-sized flow channels due to electrokinetic effects (Rice and Whitehead, 1965) and non-continuum effects, such as slip along the wall (Lim et al., 2002). However, a number of studies report increases in flow resistance in tubes as large as hundreds of micrometers in diameter (Brutin and Tadrist, 2003; Li et al., 2003; Phares and Smedley, 2004). In some of these studies, increases in flow resistance were exclusively observed in relatively rough microtubes, suggesting that this observed increase in resistance may be attributed to enhanced surface roughness effects at the microscale, even for laminar flow. Characterizing increases in flow resistance for laminar flow through microtubes is critical to understanding a number of biofluid systems that rely on efficient drainage of fluid through capillaries.

Of particular interest to the authors is the drainage of aqueous humor, a liquid resembling blood plasma, from the anterior chamber of the eye into the vascular system along the periphery of the eye. Aqueous drainage facility is known to decrease dramatically in patients who suffer from primary open angle glaucoma, but the mechanism of the increased flow resistance remains unclear. The decrease in aqueous drainage facility results in an increase in intraocular pressure (IOP), which in turn damages the optic nerve and ultimately leads to blindness. Recently, Bahler et al. (2004) observed that IOP could be decreased in cultured anterior segments of normal human eyes by using microstents to bypass part of the

* Corresponding author. Tel.: +1 979 4582264; fax: +1 979 8622418.
E-mail address: dphares@usc.edu (D.J. Phares).
[1] Present address: Department of Aerospace and Mechanical Engineering, University of Southern California, Los Angeles, CA 90089-1453, USA.

0142-727X/$ - see front matter © 2004 Elsevier Inc. All rights reserved.
doi:10.1016/j.ijheatfluidflow.2004.11.002

conventional drainage pathway. Zhou and Smedley (in press) modeled the drainage of aqueous humor in the presence of a bypass by assuming no flow resistance (i.e. no pressure drop) across the bypass. In the present work, we seek to characterize the flow resistance through well-characterized microstents of varying length and diameter for the purposes of model validation and to provide design limits in the development of future microstents. In light of the previously reported results suggesting differences between fluid flow in *long* microtubes and macrotubes, the present study focuses on characterizing any differences that may exist between flow through *short* microtubes and macrotubes.

Our approach is to measure the pressure drop across a variety of thick precision orifice plates as a function of flow rate at physiological pressures. The orifice diameters range from 80 to 150 μm and the length-to-diameter ratios (L/D) range from 2 to 5. These are similar in dimension to bypass microstents (Bahler et al., 2004). The manuscript is organized as follows. Section 2 presents the convention for describing the flow through orifices, so that similar convention may be adopted for analysis. The experimental setup and protocol are presented in Section 3 and the results of the experiments are presented in Section 4. We discuss implications of the present work to microstent design and implementation and present our conclusions in Section 5.

2. Theoretical considerations

In the absence of gravitational effects, the flow through an orifice is typically described using a discharge coefficient, C_D, a measure of entrance, exit, and frictional losses and defined (Sahin and Ceyhan, 1996):

$$C_D = \frac{Q}{A}\sqrt{\frac{\rho}{2\Delta P}}, \tag{1}$$

where Q is the flow rate, A is the cross sectional area of the orifice, ρ is the fluid density, and ΔP is the pressure drop across the orifice. For low Reynolds numbers and thick orifice plates (i.e. long tube lengths, L), the pressure gradient may be attributed mostly to frictional losses at the walls. Assuming laminar, fully-developed flow, the discharge coefficient may be derived from Poiseuille's equation:

$$Q = \frac{\Delta P \pi D^4}{128 \mu L} \tag{2}$$

yielding:

$$C_D = \left(\frac{1}{8}\sqrt{\frac{D}{L}}\right)\sqrt{Re}, \tag{3}$$

where $Re = \frac{\rho \bar{v} D}{\mu}$, D is the orifice diameter, $\bar{v}$ is the average velocity of the fluid, and μ is the dynamic viscosity. A linear relation between C_D and $\sqrt{Re}$ also exists at low Reynolds numbers for thin-plate orifices ($L/D < 1$) (Kiljanski, 1993; Sahin and Ceyhan, 1996; Borutzky et al., 2002), but deviates from the Poiseuille-based expression. Fig. 1 displays some numerical and experimental results (Johansen, 1930; Sahin and Ceyhan, 1996) for $L/D = 1/16$ and $L/D = 1$ as compared to Eq. (3). It is expected that a model based on the fully-developed flow assumption should not agree with data obtained from thin-plate orifices. However, Fig. 1 suggests that the data converge to the fully-developed solution for increasing values of L/D and decreasing values of Re and therefore implies that it may be possible to compare the flow resistance through the short microtubes in this study to Eq. (3) at low Reynolds numbers.

The validity of Eq. (3) for short microtubes requires that the entrance length be significantly smaller than the length of the tube. The dimensionless entrance length, ξ, for an initially uniform laminar flow in a circular tube was reported by Mohanty and Asthana (1978) to be:

$$\xi = \frac{x}{DRe} = 0.075. \tag{4}$$

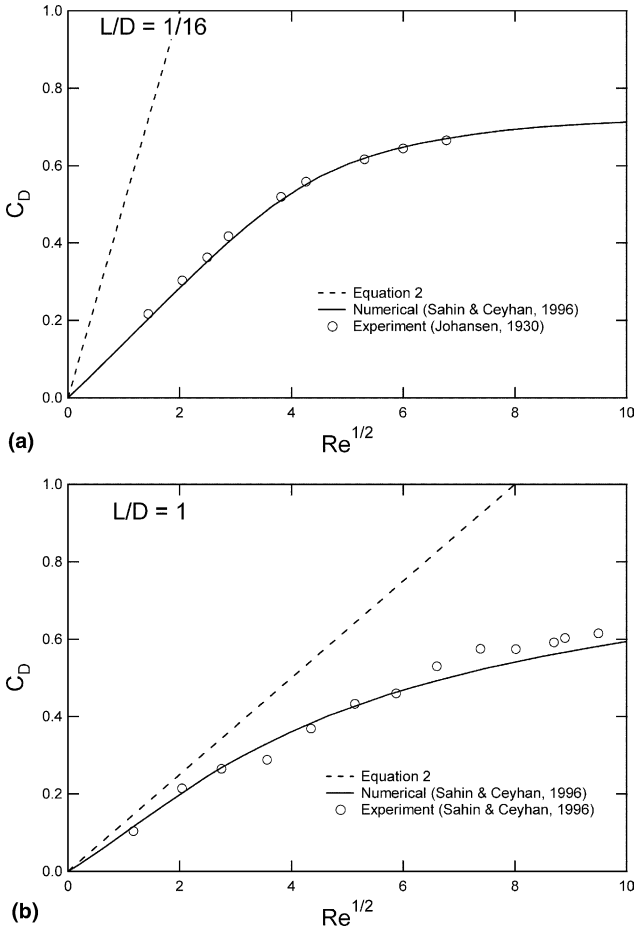

Fig. 1. Numerically and experimentally obtained discharge coefficients for thin-plate orifices compared with Poiseuille flow (Eq. (3)).

One may estimate a range of validity of Eq. (3) by setting the entrance length to be smaller than the tube length by an order of magnitude (i.e., 10% of the tube length), which by Eq. (4) yields:

$$\frac{L}{D} > 0.75Re. \tag{5}$$

One might assume other percentages; however, this value is chosen for the sake of discussion and will be tested for microtubes later in this manuscript when results of the present study are compared to Poiseuille flow. We note that Mohanty and Asthana (1978) state that Eq. (4) likely becomes inaccurate for $Re < 500$, corresponding to a critical tube length of $L/D = 375$. By contrast, we are interested in smaller Reynolds numbers and aspect ratios. In the present study, we present our results in terms of a discharge coefficient and experimentally determine under what flow conditions Eq. (3) may be applied to flow through short microtubes.

Flow through orifices with aspect ratios comparable to the present work ($L/D > 1$) was studied experimentally by Ramamurthi and Nandakumar (1999), but for Reynolds numbers greater than 2000. The authors of that study also present their results in terms of a discharge coefficient. For a 300 μm diameter orifice, C_D appeared to level off between 0.60 and 0.90 for $1 < L/D < 10$.

3. Experiments

3.1. Flow experiments

The experimental setup (Fig. 2) consists of a Cole-Palmer 74900 series syringe pump, a 0.2 μm inline filter, an Omega PX26-001GV differential pressure transducer with 0.2% repeatability, and a 1.3 cm diameter orifice plate in a flow cell that seals the plate edge on the inlet and outlet sides, securing it at the center of the holder length. Two types of orifices were employed-stainless steel precision apertures (Ladd Research) and home-made polyimide apertures. All of the orifices were subsequently analyzed by SEM to determine diameter and surface roughness, as described in the next section. The geometry involving a large and sudden change in diameter from flow in the plate holder to flow through the aperture was selected to provide a uniform velocity profile at the microtube entrance.

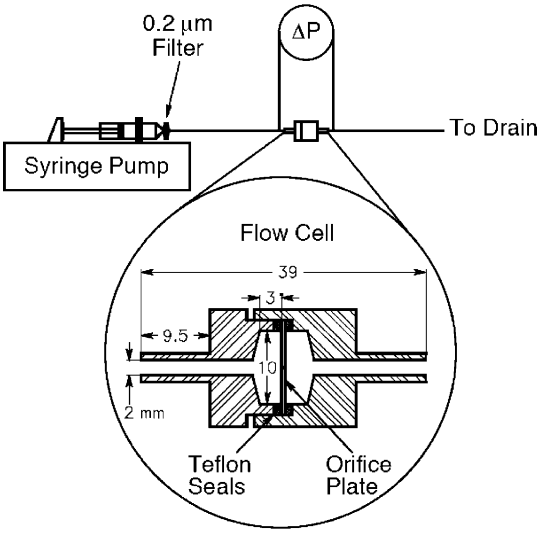

Fig. 2. Schematic of experimental setup.

The syringe pump and pressure transducer were interfaced to a PC and automated using LabView software. After all air bubbles were carefully removed from the system, the pump was commanded to step through flow rates from the minimum to the maximum and then step back down, filling in intermediate points. For each flow rate, a zero-flow pressure measurement was recorded prior to starting the pump. When the pump was turned on the pressure was allowed to stabilize before any pressure was recorded. The pressure was subsequently recorded over a period of 10 min at a sampling rate of 1000 Hz. The data during this time were recorded as an average value and a standard deviation, providing error bars for each data point. The pump was then turned off and the system allowed to equilibrate in preparation for the next zero-flow pressure reading. The final pressure drop was taken to be the difference between the recorded pressure reading and the zero-flow reading, thus eliminating any gravitational effects caused by orientation of the orifice plate or pressure transducer. Although all reported pressures correspond to the pressure difference between the inlet and outlet of the flow cell (as shown in Fig. 2), the pressure drop across the tubing associated with the flow cell accounts for less than 0.01% of the pressure drop across the microtube. Thus we assume for the subsequent analysis that the microtube accounts for the entire drop in pressure.

3.2. Orifice characterization

We employ an orifice characterization technique similar to that described by Phares and Smedley (2004) for long microtubes. Upon completion of the flow experiments, both sides of each orifice were imaged using a Scanning Electron Microscope. It is clear from the SEM images displayed in Fig. 3 that the inside wall of the tube is sharp, enabling an automated image processing scheme to determine the diameter at a variety of angular positions and calculating a mean diameter and and relative roughness. The image analysis procedure for a single image was described in a previous paper (Phares and Smedley, 2004). The results of this analysis are listed in Table 1. The stainless steel apertures,

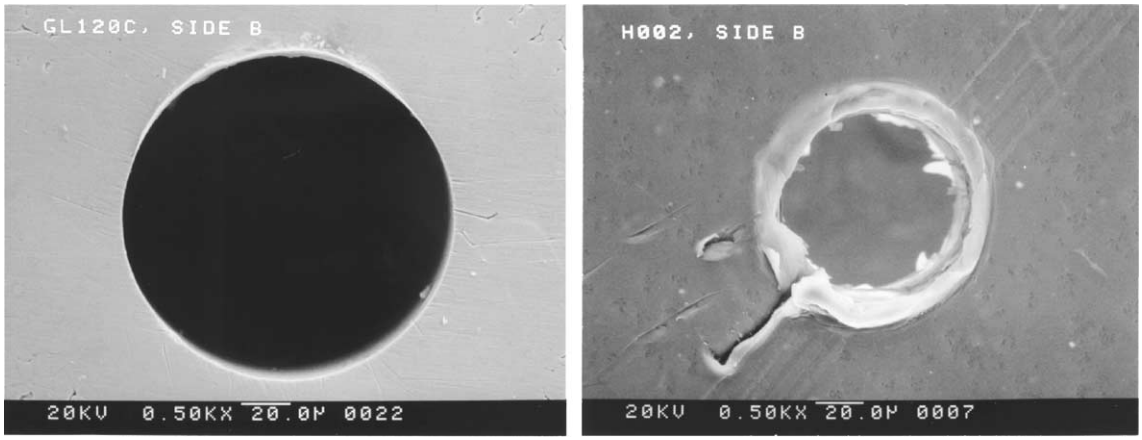

Fig. 3. SEM images of stainless steel (left) and polyimide (right) apertures. The left image is sample 7 and the right image is sample 8.

Table 1
Results of analysis of SEM images of apertures

Sample	Material	Measured length (μm)	Measured diameter (μm)	L/D	Relative roughness
1	Stainless steel	422 ± 6	81.7 ± 1.0	5.16 ± 0.10	–
2	Stainless steel	422 ± 6	99.6 ± 1.0	4.24 ± 0.07	–
3	Stainless steel	318 ± 6	129.1 ± 1.0	2.46 ± 0.05	–
4	Stainless steel	422 ± 6	130.7 ± 1.0	3.23 ± 0.05	–
5	Stainless steel	478 ± 6	129.9 ± 1.0	3.68 ± 0.05	–
6	Stainless steel	490 ± 6	128.0 ± 1.0	3.83 ± 0.06	–
7	Stainless steel	422 ± 6	159.2 ± 1.0	2.65 ± 0.04	–
8	Polyimide	386 ± 6	77.2 ± 1.0	5.00 ± 0.10	11%
9	Polyimide	381 ± 6	142.8 ± 1.0	2.67 ± 0.05	4.1%
10	Polyimide	305 ± 6	123.6 ± 1.0	2.47 ± 0.05	3.4%
11	Polyimide	531 ± 6	121.6 ± 1.0	4.37 ± 0.06	5.5%

The length uncertainty reflects the precision of the micrometer used to measure the orifice plate thickness. The diameter uncertainty reflects repeatability of multiple diameter measurements from the same SEM image.

micromachined by Ladd Research, were found to be very smooth compared to the polyimide apertures, which were fabricated in-house using a specialized high-speed drill press; presumably due in part to the gummy material properties of polyimide. The geometry of the tube inlet likely affects the entrance length of the laminar flow. We should note that the curvature radii of the entrance and exit edges were estimated by the manufacturer to be on the order of a micron. In light of the difficulties associated with machining at the microscale and the fact that the curvature radii comprise less than 1% of the tube diameters and lengths, we consider the stainless steel tube entrances to be nominally sharp-edged.

4. Results

4.1. Effect of tube diameter

Fig. 4 displays the raw data obtained from at least two separate experiments performed on each of four different tube diameters, nominally 80, 100, 130, and 160 μm (samples 1, 2, 4, and 7, respectively), and having a common length of 422 μm. The working fluid for each case is deionized water. Every experiment exhibits good repeatability, within the accuracy limits caused by the small fluctuations in the syringe pump and denoted by the error bars. For each tube diameter, the pressure drop increases linearly with flow rate for small flow rates, and then exhibits a stronger flow rate dependence beyond a threshold flow rate that increases with tube diameter. The same data are plotted in Fig. 5 as discharge coefficient, C_D, versus the square root of the Reynolds number. The linear portion of each data set agrees well with Eq. (3), which is derived from the assumption that all losses may be attributed to frictional resistance caused by a fully-developed flow. This validates the implications of Fig. 1 that the discharge coefficient may be compared to Eq. (3) for $L/D > 1$ at low Reynolds numbers. According to Fig. 5, the data begin to deviate from Eq. (3) when $\sqrt{Re} > 4$ for the smallest aspect ratio tested ($L/D = 2.65$). This deviation corresponds to a decrease in C_D, and thus an increase in the flow resistance from the purely fully-developed flow assumption.

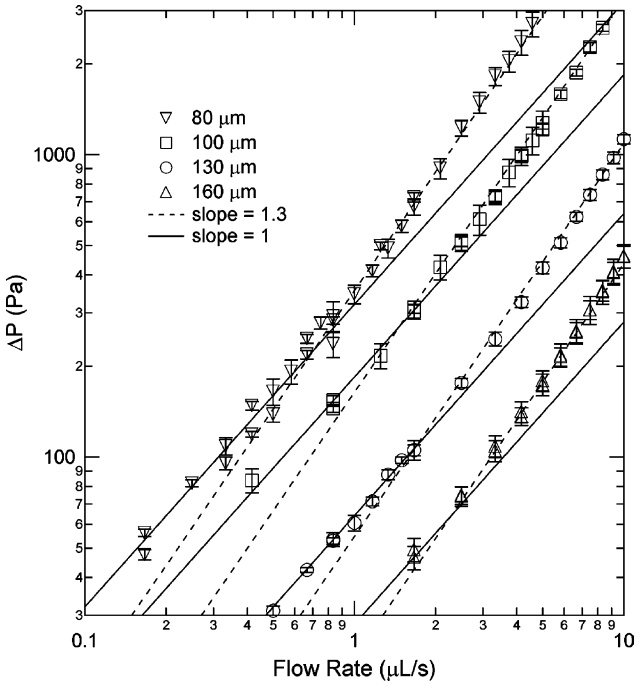

Fig. 4. Raw data for stainless steel microtubes with four different diameters.

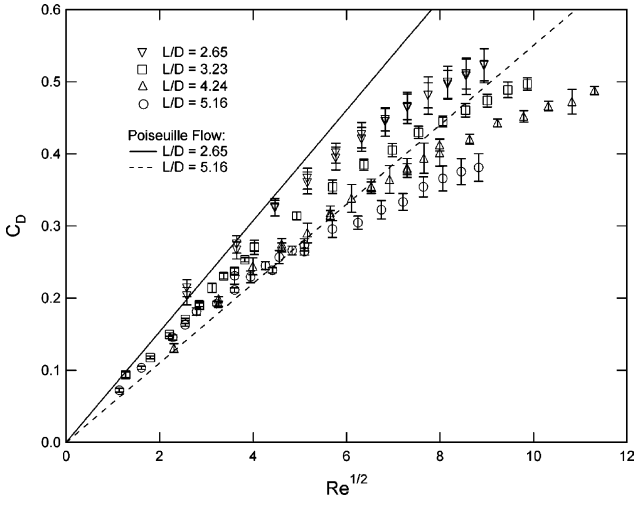

Fig. 5. Effect of microtube diameter on discharge coefficient for water flowing through stainless steel microtubes ($L = 422$ μm).

4.2. Effect of tube length

Fig. 6 displays the data obtained from similar experiments on four different tube lengths (orifice plate thicknesses) using samples 3, 4, 5, and 6. All of the tubes have similar diameters ($D \approx 130$ μm), allowing direct comparison between the pressure gradients across the tube and the Poiseuille flow solution, represented by the solid line in Fig. 6. In each case, the data appear to coincide with Poiseuille flow at flow rates less than roughly 1.7 μL/s.

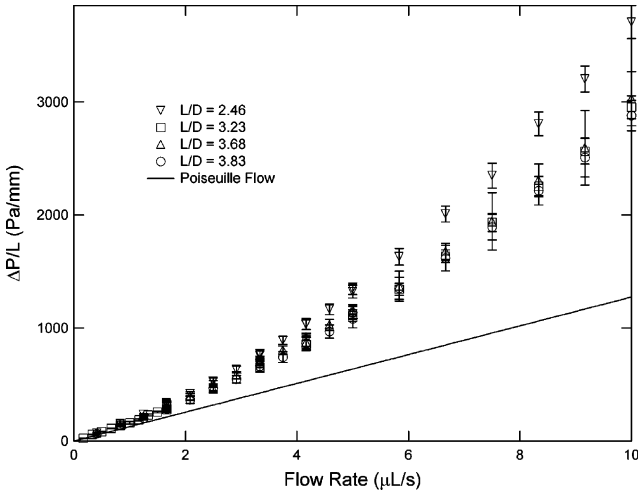

Fig. 6. Pressure gradient for stainless steel microtubes ($D = 130$ μm) with four different lengths compared with Poiseuille flow (i.e., $\frac{\Delta P}{L} = \frac{128\mu}{\pi D^4} Q$).

Beyond this flow rate, the entrance length begins to dominate the length of the tube causing deviations from the fully-developed flow solution. A notable feature of Fig. 6 is the noticeably larger pressure gradient produced by the shortest tube ($L/D = 2.46$), even as compared to the next shortest tube ($L/D = 3.23$). An explanation for this rather abrupt increase in flow resistance is a coupling between the entrance flow and the exit. Such a coupling would not be expected to exist for longer tube lengths.

4.3. Effect of fluid viscosity

In order to measure the flow resistance at smaller Reynolds numbers, we have repeated the experiments on samples 3, 4, 5, and 6 using a roughly 50/50 by volume glycerol/water solution. The dynamic viscosity of the solution was measured using a falling ball viscometer to be 7.9×10^{-3} Pa s at 21.7 °C. Although the same solution was used for each sample, the viscosity varied by roughly 6% throughout the experiments due to temperature fluctuations. Since the temperature was recorded during each experiment, the temperature sensitivity was taken into account in the data analysis. The results of these experiments are displayed in Fig. 7, along with the corresponding predictions from Eq. (3). A linear relationship is observed for each tube, as expected for the low Reynolds numbers inherent to the flows.

The agreement between all of the data with Eq. (3) at low Reynolds numbers suggests that a slightly modified scaling may be used to present the data for short microtubes, as opposed to that used for orifices. More specifically, one may expect a better collapse of the data if the discharge coefficient were plotted against $Re^{1/2}(L/D)^{-1/2}$, since the dependence on aspect ratio would be removed according to Eq. (3). Fig. 8 presents all of the

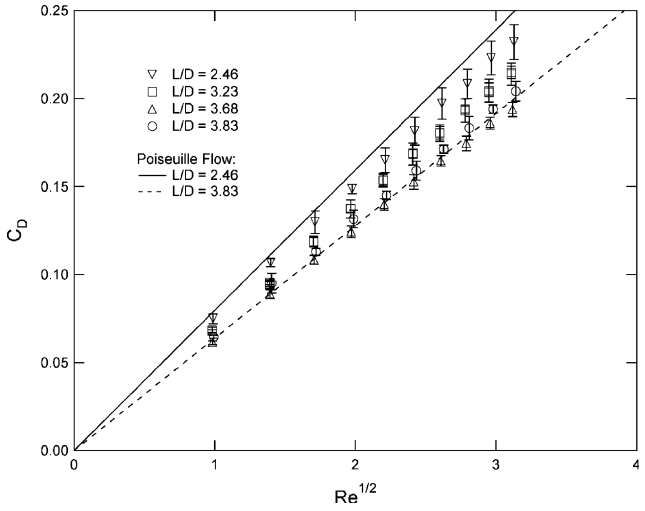

Fig. 7. Effect of microtube length on discharge coefficient for glycerol/water solution flowing through stainless steel microtubes ($D = 130$ μm).

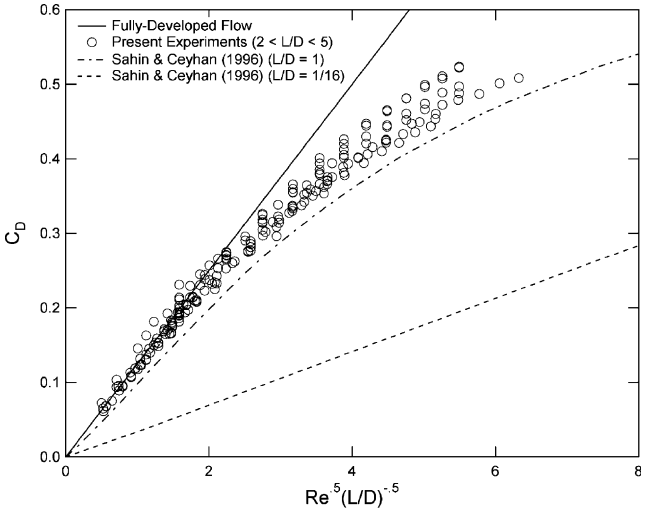

Fig. 8. All data plotted versus scaling more suited to a fully-developed flow.

data plotted using this scaling for both water and the glycerol/water solution. Indeed, the data collapse in the linear portion of the curve, and the collapse breaks down as the data deviate from the fully-developed flow solution. The collective data sets exhibit a deviation from the fully-developed flow solution at $Re^{1/2}(L/D)^{-1/2} \approx 2.25$. This provides the low Reynolds number analog to Eq. (5):

$$\frac{L}{D} > 0.20Re. \tag{6}$$

Eq. (6) represents the aspect ratio criterion for applying the assumption of fully-developed flow throughout the entire tube. We note that this implies an entrance length that is significantly shorter than what is generally accepted for higher Reynolds number laminar flows, where boundary layer analyses are sufficient in characterizing entrance regions (Mohanty and Asthana, 1978).

4.4. Effect of surface roughness

Fig. 9 displays the results for flow of a different glycerol/water solution with a measured dynamic viscosity of 9.5×10^{-3} Pa s through the rough polyimide tubes (samples 8, 9, 10, and 11) plotted using the same scaling deemed suitable for $Re^{1/2}(L/D)^{-1/2} < 2.25$, and compared with results from the smooth stainless steel tubes. As listed in Table 1, the relative surface roughness of the polyimide tubes was determined from analysis of the SEM images to vary between 3% and 11%. Even at these low Reynolds numbers, the data appear to deviate from the fully-developed flow solution, corresponding to lower discharge coefficients, and thus larger resistance to flow. Although it may appear that the increase in flow resistance scales better with aspect ratio than relative surface roughness, the two are coupled since roughness may affect the length of the entry region. Furthermore, we are unable to determine the longitudinal structure of the surface elements from the images of the cross sections. Thus, no quantitative relation between flow resistance and surface roughness should be extracted from the data. A more quantitative study of the effect of surface roughness would require a more accurate determination of surface topography using an atomic force microscope or optical profilometer.

Hasegawa et al. (1997) performed similar experiments on the flow of water, glycerin, and silicon oil through microorifices ($L/D < 1.14$) and also observed increases in flow resistance, but only for orifices smaller than

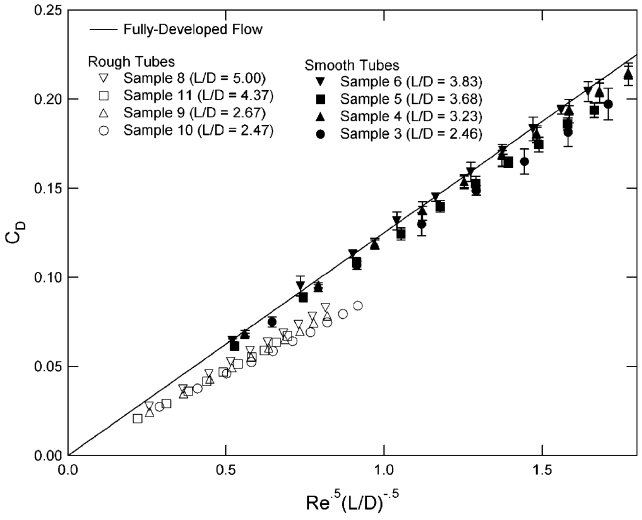

Fig. 9. Discharge coefficient plotted for glycerol/water mixture flowing through polyimide apertures with varying lengths and diameters compared with stainless steel apertures. We have omitted error bars on the open symbols because they are smaller than the size of the symbols.

65 μm in diameter. The authors of that study ruled out electrokinetic effects by repeating the experimental results using a concentrated saline solution. They also used a numerical analysis to rule out the effect of a bur, 7% the size of the orifice diameter, located on the leading edge of the orifice. The bur constructed for numerical analysis did not protrude into the orifice, but rather extended out from the face of the orifice plate. In the present study, it may be more reasonable to attribute the increase in flow resistance in the polyimide samples to surface roughness because the surface structures appear to extend into the orifice (see Fig. 3). For a relevant numerical study of a similar geometry, we refer the reader to Lee (2002), who examined the effect of tube constrictions for Reynolds numbers between 5 and 400.

5. Discussion and conclusions

The agreement with the fully-developed flow assumption for the smooth microtubes suggests no measurable difference from flow through short smooth macrotubes for $Re < 5(L/D)$. However, the increase in flow resistance through the rough tubes resembles that observed by Li et al. (2003) and Phares and Smedley (2004) in long rough microtubes. In those studies, the flow was found to be sensitive to relative surface roughness as small as 3% in tubes smaller than several hundred micrometers in diameter and for low Reynolds numbers. This represents a significant deviation from what is generally accepted for laminar flow in macrotubes. The present results exhibit a similar sensitivity of the flow resistance to the relative surface roughness, but the authors are unaware of any studies of the effect of surface roughness on low Reynolds number flow through short macrotubes. Therefore, no direct comparisons may be made at the present time to determine whether the observed sensitivity to surface roughness may be attributed to the scale of the experiments.

Our measurements of the pressure drop across short microtubes suggest a scaling law that is a departure from the typical orifice scaling. For smooth microtubes, the data collapse to a line at small Reynolds numbers (determined by Eq. (6)) in a manner that is consistent with fully-developed flow throughout the length of the tube. Although we have not verified that the flow is actually fully-developed, the results at least provide an empirical predictive tool for flow through straight, sharp-edged microtubes. On a practical basis, the data suggest that calculations based on the Poiseuille equation are suitable at physiological flow rates for microstents with aspect ratios as small as $L/D = 2$. Flow resistance also appears to be sensitive to relative surface roughness. This sensitivity has been observed in long microtubes as well, but it is unclear whether the same mechanism is responsible.

References

Bahler, C.K., Johnson, D.H., Smedley, G.T., 2004. Trabecular bypass stents increase outflow facility in cultured human anterior segments. Abstract 4384, Annual meeting of the Association for Research in Vision and Ophthalmology.

Borutzky, W., Barnard, B., Thoma, J., 2002. An orifice flow model for laminar and turbulent conditions. Simul. Modell. Practice Theory 10, 151.

Brutin, D., Tadrist, L., 2003. Experimental friction factor of a liquid flow in microtubes. Phys. Fluids 15, 653.

Hasegawa, T., Suganuma, M., Watanabe, H., 1997. Anomaly of excess pressure drops of the flow through very small orifices. Phys. Fluids 9, 1.

Johansen, F.C., 1930. Flow through pipe orifices at low Reynolds number. Proc. R. Soc. 126, 231.

Kiljanski, T., 1993. Discharge coefficient for free jets from orifices at low Reynolds number. J. Fluids Eng. 115, 778.

Kulinsky, L., Wang, Y., Ferrari, M., 1999. Electroviscous effects in microchannels. Proc. SPIE 3606, 158.

Lee, T.S., 2002. Numerical study of fluid flow through double bell-shaped constrictions in a tube. Int. J. Numer. Methods Heat Fluid Flow 12, 258.

Li, Z., Du, D., Guo, Z., 2003. Experimental study on flow characteristics of liquid in circular microtubes. Microscale Thermophys. Eng. 7, 25.

Lim, C.Y., Shu, C., Niu, X.D., Chew, Y.T., 2002. Application of lattice Boltzmann method to simulate microchannel flows. Phys. Fluids 14, 2299.

Mala, G.M., Li, D., 2000. Flow characteristics of water in microtubes. Int. J. Heat Mass Transf. 20, 1165.

Mohanty, A.K., Asthana, S.B.L., 1978. Laminar-flow in the entrance region of a smooth pipe. J. Fluid Mech. 90, 433.

Phares, D.J., Smedley, G.T., 2004. A study of laminar flow of polar liquids through circular microtubes. Phys. Fluids 16, 1267.

Ramamurthi, K., Nandakumar, K., 1999. Characteristics of flow through small sharp-edged cylindrical orifices. Flow Meas. Instrum. 10, 133.

Ren, L., Li, D., Qu, W., 2001. Electro-viscous effects on liquid flow in microchannels. J. Colloid Interface Sci. 233, 12.

Rice, C.L., Whitehead, R., 1965. Electrokinetic flow in a narrow cylindrical capillary. J. Phys. Chem. 69, 4017.

Sahin, B., Ceyhan, H., 1996. Numerical and experimental analysis of laminar flow through square-edged orifice with variable thickness. Trans. Inst. Meas. Control 178, 166.

Zhou, J., Smedley, G.T., 2004. A trabecular bypass flow model. J. Glaucoma, in press.